

RESEARCH ARTICLE

10.1002/2014JF003193

Key Points:

- Evaluation of slope stability from WL shear strength spatial variability
- Quantification of the knock-down effect on stability due to spatial variability
- Derivation of the critical length from the heterogeneous FE simulations

Supporting Information:

- Readme
- Movie S1
- Movie S2

Correspondence to:

J. Gaume,
gaume@slf.ch

Citation:

Gaume, J., J. Schweizer, A. van Herwijnen, G. Chambon, B. Reuter, N. Eckert, and M. Naaim (2014), Evaluation of slope stability with respect to snowpack spatial variability, *J. Geophys. Res. Earth Surf.*, 119, 1783–1799, doi:10.1002/2014JF003193.

Received 13 MAY 2014

Accepted 16 AUG 2014

Accepted article online 21 AUG 2014

Published online 17 SEP 2014

Evaluation of slope stability with respect to snowpack spatial variability

J. Gaume¹, J. Schweizer¹, A. van Herwijnen¹, G. Chambon^{2,3}, B. Reuter¹, N. Eckert^{2,3}, and M. Naaim^{2,3}

¹WSL Institute for Snow and Avalanche Research SLF, Davos, Switzerland, ²UR ETGR, IRSTEA, Grenoble, France,

³Université Grenoble Alpes, Grenoble, France

Abstract The evaluation of avalanche release conditions constitutes a great challenge for risk assessment in mountainous areas. The spatial variability of snowpack properties has an important impact on snow slope stability and thus on avalanche formation, since it strongly influences failure initiation and crack propagation in weak snow layers. Hence, the determination of the link between these spatial variations and slope stability is very important, in particular, for avalanche public forecasting. In this study, a statistical-mechanical model of the slab-weak layer (WL) system relying on stochastic finite element simulations is used to investigate snowpack stability and avalanche release probability for spontaneously releasing avalanches. This model accounts, in particular, for the spatial variations of WL shear strength and stress redistribution by elasticity of the slab. We show how avalanche release probability can be computed from release depth distributions, which allows us to study the influence of WL spatial variations and slab properties on slope stability. The importance of smoothing effects by slab elasticity is verified and the crucial impact of spatial variation characteristics on the so-called knock-down effect on slope stability is revisited using this model. Finally, critical length values are computed from the simulations as a function of the various model parameters and are compared to field data obtained with propagation saw tests.

1. Introduction

Evaluating avalanche release conditions is crucial for both public forecasting and avalanche hazard mapping. Most avalanche incidents are caused by dry snow slab avalanches which generally result from a sequence of fracture processes including (1) failure initiation in a weak snow layer underlying a cohesive slab, (2) crack propagation within the weak layer, and (3) slab tensile fracture which leads to its detachment [McClung, 1979; Schweizer *et al.*, 2003]. Due to the multiscale variability of the quantities involved in avalanche release and the complex microstructure of snow, accurate prediction of location and timing of snow avalanches is so far not possible. For instance, snowfall and snow depth are highly variable at the mountain range and regional scale [Durand *et al.*, 2009; Blanchet and Lehning, 2010; Eckert *et al.*, 2010; Gaume *et al.*, 2013b] and mechanical properties of snow are strongly heterogeneous at the basin and slope scale [e.g., Jamieson and Johnston, 2001; Kronholm and Schweizer, 2003; Schweizer *et al.*, 2008]. This spatial variability is due to several external drivers such as precipitation, wind or solar radiation, and their interaction with terrain and also to internal processes such as snow metamorphism or water infiltration. Understanding and predicting avalanche release under such multiscale spatial variations is extremely complex, and they hinder deterministic modeling of avalanche release.

Numerous field studies have documented spatial variations of snow cover properties to investigate the reliability of snow slope stability measurements [e.g., Jamieson and Johnston, 1993; Birkeland *et al.*, 1995; Landry *et al.*, 2004]. More recently, it was recognized that these spatial variations play an important role in the fracture processes of failure initiation and crack propagation in the weak layer leading to dry snow slab avalanche release [Schweizer *et al.*, 2008]. However, the link between snowpack spatial variability and slope stability has still not been fully established [Bellaire and Schweizer, 2011] and is currently still a topic of active research [Reuter and Schweizer, 2013].

Hence, to investigate slope stability and avalanche release size, measured variations in snow properties have been used as input for numerical models of slab-weak layer systems [Failletaz *et al.*, 2004; Fyffe and Zaiser, 2004, 2007; Chiaia and Frigo, 2009; Gaume *et al.*, 2012, 2013a]. By coupling results of a mechanical model accounting for variations in the mechanical properties of the weak layer with observed snowfall

distributions, *Gaume et al.* [2012, 2013a] were able to reproduce avalanche release depth distributions from field observations which proved to be very useful for long-term hazard mapping, for instance, using statistical-dynamical simulations [*Meunier and Ancey*, 2004; *Eckert et al.*, 2010]. These results thus confirmed the major influence played by the heterogeneity of weak layer mechanical properties on avalanche release size.

Our aim is therefore to relate snowpack variability and slope stability for natural releases by using a mechanically-based statistical model of avalanche release. The model, based on the stochastic finite element method, was initially developed to compute avalanche release depth distributions required as input of avalanche flow models for hazard mapping [*Gaume et al.*, 2012, 2013a]. In this paper, we extended it to focus on the avalanche release probability as a function of snowpack properties and their spatial variations, in view of avalanche forecasting.

We will first present the method used to compute the avalanche probability from release depth distributions. Then, we will show how slope stability is influenced by variations of weak layer (WL) mechanical properties in terms of average shear strength, its standard deviation, and correlation length. The influence of slab properties on the results, in terms of slab thickness and elastic modulus will also be presented. Furthermore, these results will be applied to a case study of a virtual snow slope to highlight the importance of considering spatial variability for practical applications such as public avalanche forecasting. Finally, we will show how to compute the critical length required for a self-propagating crack as a function of the model parameters. The modeled critical lengths will then be compared to the ones obtained from propagation saw tests.

2. Methods

2.1. Presentation of the Mechanically-Based Statistical Model

The mechanically-based statistical model developed by *Gaume et al.* [2012, 2013a] enables finite element simulations of a slab-WL system. The model takes into account the spatial variations of snowpack mechanical properties and stress redistribution effects by the elasticity of the slab.

The weak layer is modeled as quasi-brittle (strain softening) interface with a Mohr-Coulomb failure criterion characterized by a cohesion c and a friction angle $\phi = 30^\circ$ [*van Herwijnen and Heierli*, 2009]. The shear strength of the weak layer is thus equal to $\tau_p = c + \mu\sigma_n$, where $\sigma_n = \rho gh \cos \theta$ (note that values can be locally different due to stress redistributions induced by slab elasticity or to inertia) is the applied normal stress with h the slab depth (measured normal to the slope), ρ the slab density, θ the slope angle, and $\mu = \tan \phi$ the friction coefficient. The objective is not to develop a complete mechanical model of slab avalanche release accounting for all the complex processes at play. Both the geometry and the mechanical behavior of the system are greatly simplified while keeping the ingredients essential to describe the mechanics of snow slab release in order to relate slope stability to weak layer heterogeneity. Note, however, that the results of this study would still remain relevant if a different mode of WL failure, such as suggested in the anticrack model [*Heierli et al.*, 2008], would be assumed, as discussed in Appendix B and in section 4.

The spatial variability is accounted for through a stochastic distribution of the cohesion c of the WL with a spherical covariance function of correlation length ϵ (this covariance function is presented in more detail in *Gaume et al.* [2013a]). The average cohesion is denoted by $\langle c \rangle$, its standard deviation by σ_c , and the coefficient of variation by $CV = \sigma_c / \langle c \rangle$. The shear stiffness (interfacial shear elastic modulus in Pa/m) of the WL is denoted as k_s (see *Gaume et al.* [2013a], for more details). The homogeneous slab is elastic with a density ρ , a constant Young's modulus E (varying in a range of realistic values between 0.1 and 100 MPa, according to *Mellor* [1975], *Scapozza* [2004], and *Sigrist* [2006]) and a constant Poisson's ratio $\nu = 0.2$. The system is loaded by progressively increasing the slope angle θ until failure. Time-dependent aspects of the failure process were not taken into account as we focus on the final stage of failure which is characterized by very high strain rates. For each set of parameters (slab depth h , WL average cohesion $\langle c \rangle$, its standard deviation σ_c , and correlation length ϵ), 100 finite element simulations were performed with different realizations of the heterogeneity of the weak layer shear strength ($\tau_{p,i}(x) = c_i(x) + \mu\sigma_n$, $i = 1, \dots, 100$), leading to 100 values of the release angle so that a statistical analysis can be performed [see *Gaume et al.*, 2013a, for more details]. In total, more than 8000 finite simulations were performed. The simulated system is represented in Figure 1 with an example of WL shear strength variation.

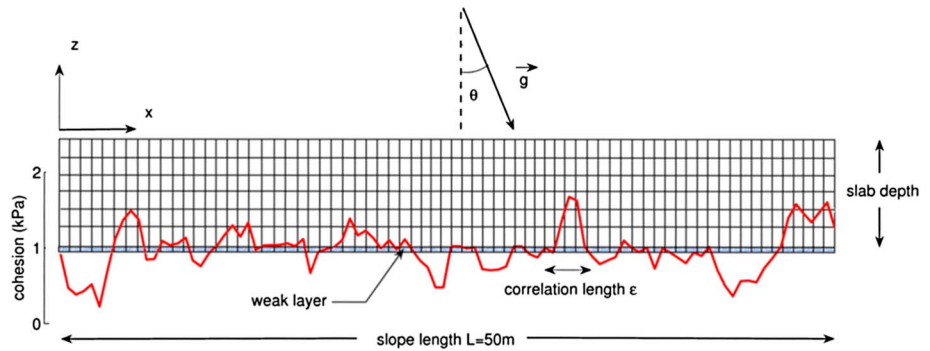


Figure 1. Configuration of the slab weak layer system. The red curve represents a realization of the Gaussian heterogeneity of the weak layer strength (cohesion) for $\epsilon = 2$ m. The system is loaded by increasing the slope angle until failure. Slab mesh: 100 elements in the x direction, six elements in the z direction. WL interface mesh: 100 elements in the x direction.

Two videos of finite element simulations with a heterogeneous WL and a single crack (also called deficit zone or super weak zone in the literature) are available as a supporting information showing the temporal evolution of the stresses inside the weak layer during loading.

2.2. Evaluation of Avalanche Release Probability

The model results were analyzed to compute for each simulation the critical release depth h_c corresponding to the mechanical stability criterion for a given slope angle. The release depth distribution $p(h_c|\theta)$ was adjusted by the following normal distribution [Gaume et al., 2013a]:

$$p(h_c|\theta) = \frac{1}{\sigma_h \sqrt{2\pi}} e^{-\frac{1}{2} \left(\frac{h_c - \langle h \rangle}{\sigma_h} \right)^2}, \quad (1)$$

with $\langle h \rangle = \langle c \rangle f_1 / (\rho g F)$ the average release depth, $\sigma_h = \sigma_c \sqrt{f_2} / (\rho g F)$ the release depth standard deviation, and $F = \sin \theta - \mu \cos \theta$. The function f_1 (always lower than 1) is called the “knock-down” function since its effect is to decrease the apparent cohesion $f_1 \langle c \rangle$ of the weak layer. As we will show, f_1 depends on the correlation length ϵ , the slab depth h , the coefficient of variation of the heterogeneity $CV = \sigma_c / \langle c \rangle$, the Young’s modulus E of the slab and the characteristic length of the system $\Lambda = \sqrt{E' h / k_s}$ associated with stress redistributions due to slab elasticity. Here $E' = E / (1 - \nu^2)$ and k_s is the weak layer shear stiffness. The function f_2 (also always lower than 1) is called the smoothing function since it decreases the apparent variability. It depends on E , ϵ , and Λ . The functions f_1 and f_2 will be presented in more detail in section 3. From equation (1), one can define an avalanche probability P_{aval} , the probability that the “real” slab depth h_{real} exceeds the critical depth h_c following from the mechanical stability criterion.

$$P_{aval} = P(h = h_{real} \geq h_c) = \int_0^h p(h_c|\theta) dh_c. \quad (2)$$

In addition, since Λ and f_1 vary only slightly with h in our results (see Gaume et al. [2013a], and section 3.1), we assume Λ to be constant in the following. This approximation does not significantly influence the results to be presented, but it allows us to obtain analytical solutions. The avalanche probability can then be rewritten as

$$P_{aval} = \frac{1}{2} \left[1 + \operatorname{erf} \left(\frac{\rho g h F - f_1 \langle c \rangle}{\sigma_c \sqrt{2 f_2}} \right) \right], \quad (3)$$

erf being the well-known error function. Our avalanche probability is a quantitative slope stability indicator depending on slab depth h , slope angle θ via F , and the variability parameters $\langle c \rangle$, σ_c , and ϵ . The avalanche probability also depends on E via f_1 and f_2 . Since the erf function increases from -1 to $+1$, and the denominator $\sigma_c \sqrt{2 f_2}$ is always positive, stability significantly depends on the sign of $\rho g h F - f_1 \langle c \rangle$. Typically, one can define two main stability cases: stable for $P_{aval} < 0.5$ and unstable for $P_{aval} > 0.5$ (Figure 2). In terms of stress and strength, one can note that analyzing the sign of $\rho g h F - f_1 \langle c \rangle$ is equivalent to analyzing the sign

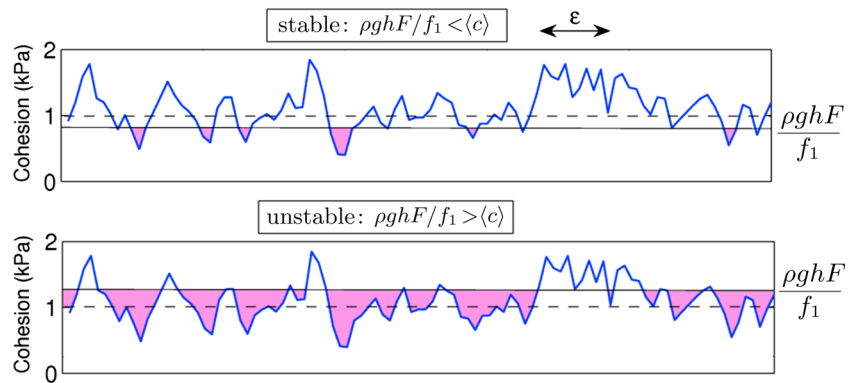


Figure 2. Schematic representation of the two main stability cases depending on the sign of the quantity $\rho ghF - f_1 \langle c \rangle$. The blue curve is an example of a realization of the cohesion heterogeneity for $\langle c \rangle = 1$ kPa (dashed line) and $\sigma_c = 300$ Pa. The zones where $\rho ghF/f_1 > c$ are colored in magenta. (top) Stable case; (bottom) unstable case.

of $\tau - \langle \tau_p \rangle^*$, the difference between the shear stress due to the slab $\tau = \rho gh \sin \theta$ and the apparent average shear strength of the WL $\langle \tau_p \rangle^* = f_1 \langle c \rangle + \mu \sigma_n$.

3. Results

In the following, we first analyze the drivers of the knock-down and smoothing functions f_1 and f_2 , respectively. Then, we show the influence of WL variability in terms of $\langle c \rangle$, σ_c , and ϵ , as well as slab elasticity on avalanche probability (equation (3)). Finally, the results will be applied to a case study of a virtual snow slope.

3.1. Knock-Down Function f_1

The knock-down function f_1 corresponds to the ratio between the average release depth $\langle h \rangle$ for a heterogeneous WL and the release depth $h_{th} = \langle c \rangle / (\rho g F)$ that would be obtained with a homogeneous WL characterized by a cohesion equal to $\langle c \rangle$. The function f_1 decreases with ϵ/h for all values of the Young's modulus (Figure 3a). If the correlation length is much smaller than slab depth, the slab "sees" the weak layer as homogeneous, which is why f_1 tends to 1. On the contrary, if the correlation length becomes larger than the slab depth, the system is sensitive to local shear strength minima which facilitate failure initiation. The function f_1 also linearly decreases with the coefficient of variation CV (Figure 3b). Indeed, variations with large amplitude lead to long zones that are weaker than the average cohesion (Figure 2) so that the apparent cohesion, product between $\langle c \rangle$ and f_1 , decreases. Overall, f_1 increases with E , for all the values of ϵ/h or CV. For a very rigid slab, f_1 is almost independent of CV and very close to 1. The stiffer the slab is, the smaller the knock-down effect becomes. A complete fitted expression of f_1 with dimensionless parameters of the system, namely, a combination between ϵ/Λ , h/Λ , $E/(\rho g \Lambda)$, and CV is detailed in Appendix A. The proposed expression allowed to explain all the data sets from the FE simulations for the different model parameters by matching all the data points on a single master curve.

In order to better understand these dependencies, the simple case of a single crack of shear strength equal to the residual stress τ_r (zero cohesion) within a homogeneous WL is examined (see section 3.4 and the illustration in the supporting information). The solution of this problem was given by Chiaia *et al.* [2008] and generalized by Gaume *et al.* [2013a] for a Mohr-Coulomb WL failure criterion, showing that a stress concentration occurs at the tip of the crack. Hence, once a crack is initiated in a very weak zone, stresses will be redistributed toward stronger neighboring areas which in turn will reach the failure criterion more easily. For a crack of half-length a , the maximum shear stress at the tip is given by

$$\tau_{\max} = \tau_g \left[1 - \frac{a}{\Lambda} \left(\frac{\tau_r}{\tau_g} - 1 \right) \right], \quad (4)$$

where $\tau_r = \sigma_n \tan \phi$ is the residual stress inside the crack and $\tau_g = \rho gh \sin \theta$ the shear stress due to the weight of the slab. The crack becomes self-propagating when this maximum shear stress reaches the failure

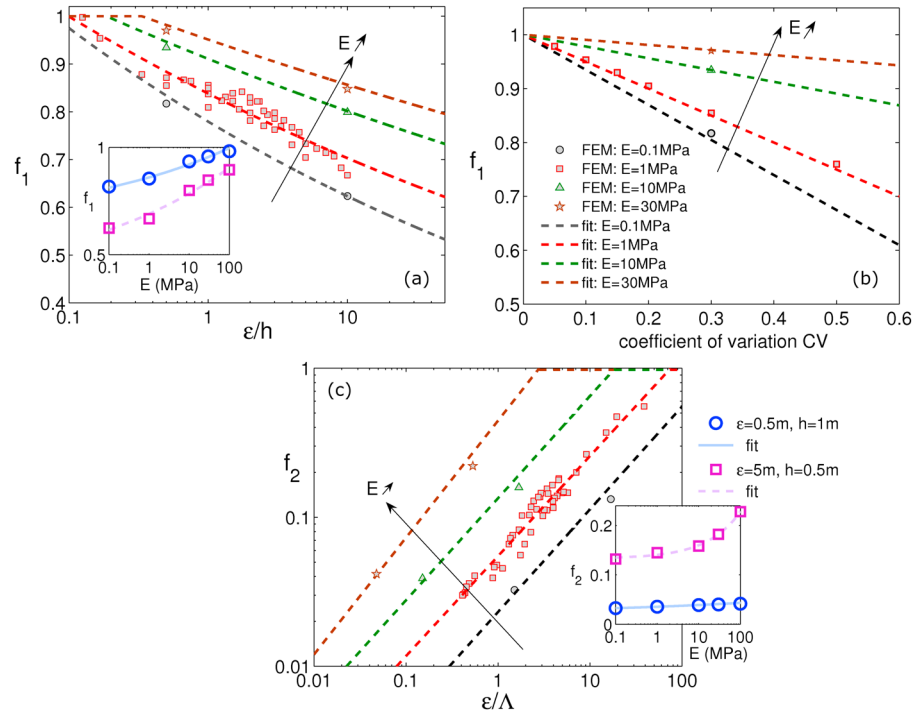


Figure 3. (a) Knock-down function f_1 versus ϵ/h for different Young's moduli E of the slab and for $CV = 30\%$. (b) Influence of the coefficient of variation CV of WL cohesion (strength) and Young's modulus on f_1 for $h = 1$ m and $\epsilon = 0.5$ m. (c) Influence of ϵ/Λ and Young's modulus on the smoothing function f_2 for $CV = 30\%$. The different colors correspond to the different values of Young's modulus (black: $E = 0.1$ MPa, red: $E = 1$ MPa, green: $E = 10$ MPa, and brown: $E = 30$ MPa). The symbols are the results from the FE model, and the dashed lines are the fitted FE results (see Appendix A). The two insets represent the dependence of f_1 and f_2 with Young's modulus for two (ϵ, h) couples: ($\epsilon = 5$ m, $h = 0.5$ m) and ($\epsilon = 0.5$ m, $h = 1$ m).

criterion. Hence, the critical shear stress $\tau_{g,s}$ required for expansion of a single crack of half-length a can be computed:

$$\tau_{g,s} = \frac{1}{1 + \frac{a}{\Lambda}} \left[c + \sigma_n \tan \phi \left(1 + \frac{a}{\Lambda} \right) \right]. \tag{5}$$

Hence, one can deduce the ratio between the release depth h and the release depth that would be obtained without the crack $h_{th} = c/(\rho g F)$ (case of a homogeneous weak layer):

$$f_1 = \frac{h}{h_{th}} = \frac{1}{1 + \frac{a}{\Lambda}}. \tag{6}$$

The origin of the dependence of f_1 on ϵ/h , CV , and E (Figures 3a and 3b) can therefore be qualitatively explained by equation (6) and the fact that potential crack lengths increase with increasing correlation length ϵ and coefficient of variation CV (Figure 2) and that Λ increases with increasing slab depth h and Young's modulus E of the slab. If $a/\Lambda \ll 1$, for instance, for small values of ϵ or CV or for high values of h or E , then f_1 tends to 1, limit which would correspond to the case of a homogeneous weak layer. On the contrary, with increasing ratio of a/Λ , the knock-down function f_1 decreases.

3.2. Smoothing Function f_2

The smoothing function f_2 corresponds to the ratio between the release depth variance σ_h^2 and the variance that would be obtained for a completely rigid slab ($E \rightarrow \infty$), in which case the stresses would exactly follow the heterogeneity variations (no stress redistribution):

$$f_2 = \frac{\sigma_h^2}{\sigma_\infty^2}, \tag{7}$$

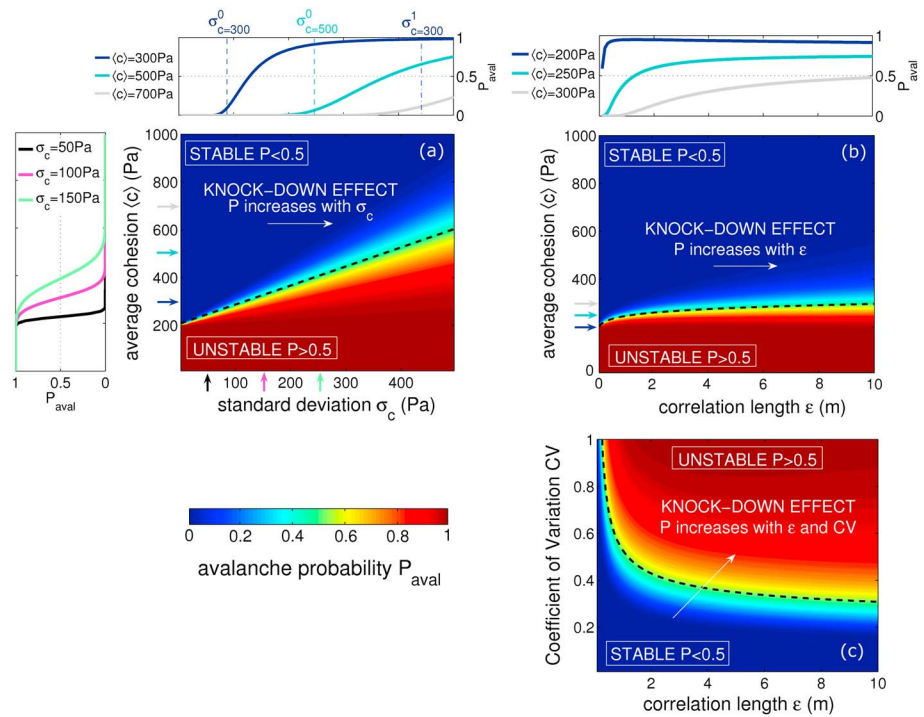


Figure 4. Avalanche probability as a function of heterogeneity parameters: (a) average WL cohesion $\langle c \rangle$ and its standard deviation σ_c for $\epsilon = 2$ m, (b) average WL cohesion $\langle c \rangle$ and correlation length ϵ for CV = 30%, and (c) coefficient of variation CV and correlation length for $\langle c \rangle = 300$ Pa. All these graphics have been computed for $h = 0.5$ m, $\rho = 250$ kg/m³, $E = 1$ MPa, and $\theta = 38^\circ$. The black dashed line corresponds to $P_{\text{aval}} = 0.5$. The marginal graphs with the white background represent 1-D plots of the avalanche probability for fixed values of one of the 2-D diagram variables (highlighted with arrows).

with $\sigma_\infty^2 = \sigma_c^2 / (\rho g F)^2$. Overall, f_2 , similar to f_1 , is always lower than 1 and increases with increasing ϵ / Λ (Figure 3c). When the correlation length is much smaller than the characteristic elastic length of the system, the variability is smoothed by the elasticity of the slab and thus the apparent (or “smoothed”) standard deviation $\sigma_c \sqrt{2f_2}$ tends to 0. This smoothing is further amplified by the elasticity of the slab, explaining the increase of f_2 with increasing E . Similarly as for f_1 , the complete relation between f_2 and the dimensionless parameters ϵ / Λ and $E / (\rho g \Lambda)$ fitted by a single function is detailed in Appendix A.

3.3. Influence of Weak Layer Spatial Variability on Slope Stability

Substituting the fitted knock-down and smoothing functions f_1 and f_2 (Appendix A) into equation (3) allowed us to calculate the avalanche probability P_{aval} as a function of the parameters that characterize the variability of the WL (Figure 4) and as a function of Young’s modulus (Figure 5).

3.3.1. Influence of the Average Cohesion

As expected, the avalanche probability decreases with increasing $\langle c \rangle$ for all values of σ_c (Figure 4a) and ϵ (Figure 4b). For $\sigma_c = 0$ (case of a homogeneous WL, $f_1 = 1$) P_{aval} goes abruptly from 1 to 0 for $\langle c \rangle = \rho g h F$. As σ_c increases, the decrease of P_{aval} with $\langle c \rangle$ is smoother and a higher value of $\langle c \rangle$ is required to reach complete stability ($P_{\text{aval}} = 0$). The average cohesion value from which P_{aval} starts to decrease is always the same, i.e., $\langle c \rangle = \rho g h F$, independent of σ_c . The limit between stable ($P_{\text{aval}} < 0.5$) and unstable regions ($P_{\text{aval}} > 0.5$) is defined by the criterion $\rho g h F = f_1(\langle c \rangle)$. Therefore, for a heterogeneous WL ($f_1 < 1$), a value of $\langle c \rangle$ higher than the homogeneous value $\rho g h F$ is required to stabilize the system, i.e., cross the $P_{\text{aval}} = 0.5$ line.

3.3.2. Influence of the Cohesion Standard Deviation

The avalanche probability generally increases with increasing standard deviation σ_c for all values of the average cohesion $\langle c \rangle$. This clearly illustrates the knock-down effect on slope stability caused by variations in WL shear strength. This effect thus causes lower release depths than in the case of a homogeneous WL due to a decrease in stability.

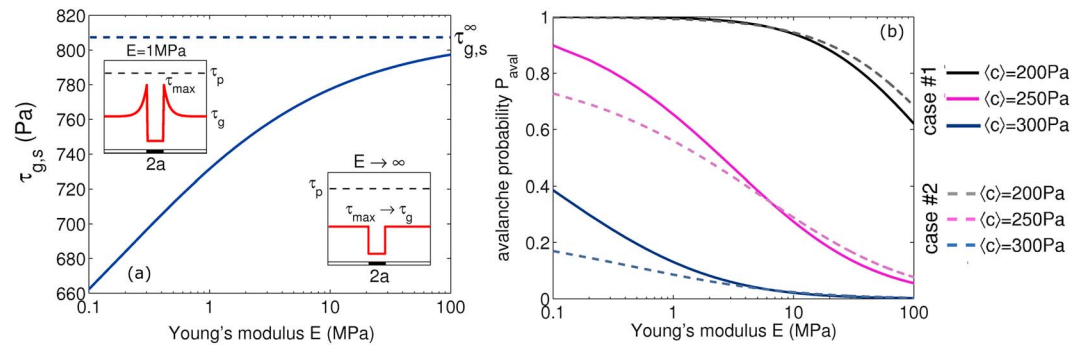


Figure 5. (a) Critical body weight shear stress required for propagation of a preexisting crack versus Young's modulus E of the slab. The crack has a half-length $a = 0.5$ m, a slope angle of $\theta = 38^\circ$, a slab density of $\rho = 250$ kg/m³, and depth $h = 0.5$ m. The insets show the shear stress profiles around the crack for an elastic ($E = 1$ MPa) and a rigid slab ($E \rightarrow \infty$). (b) into versus Young's modulus E for different average WL cohesion. Two cases are shown: #1 constant load and constant slab density $\rho = 250$ kg/m³ (solid lines) and #2 same load but with a density obtained from Young's modulus via Scapozza [2004]'s adjustment (equation (10)) and a slab depth inversely proportional to the density.

In detail, the initial value of σ_c at which P_{aval} clearly starts to increase from zero depends on $\langle c \rangle$. This value, denoted by σ_c^0 , corresponds to the amount of variability required to reach locally the stress value ρghF . If the entire cohesion distribution is above ρghF , then $P_{\text{aval}} = 0$. The value of σ_c^0 can be approximated by

$$\sigma_c^0 = \frac{f_1 \langle c \rangle - \rho ghF}{1.96 \sqrt{f_2}}, \quad (8)$$

since 95% of the apparent cohesion values belong to $[f_1 \langle c \rangle - 1.96 \sigma_c \sqrt{f_2}; f_1 \langle c \rangle + 1.96 \sigma_c \sqrt{f_2}]$ if c is simulated through a Gaussian process. Two σ_c^0 values are shown by the vertical dotted lines for $\langle c \rangle = 300$ Pa and $\langle c \rangle = 500$ Pa in Figure 4a (top). On the contrary, to reach instability, if the overall cohesion distribution is below ρghF , a certain value of the standard deviation σ_c^1 is required and defined by

$$\sigma_c^1 = \frac{f_1 \langle c \rangle + \rho ghF}{1.96 \sqrt{f_2}}. \quad (9)$$

For the case $\langle c \rangle = 300$ Pa, the corresponding value of σ_c^1 is shown in Figure 4a (top) by a dash-dotted line.

3.3.3. Influence of the Cohesion Correlation Length

The avalanche probability P_{aval} generally increases with ϵ (Figure 4b). The rate of increase as well as the limit value of P_{aval} for a high value of the correlation length depend on the average cohesion. For instance, for $\langle c \rangle \geq 300$ Pa (grey line in Figure 4b, top), the avalanche probability remains below 0.5. Consequently, the correlation length also has a knock-down effect on slope stability, albeit less pronounced than the effect of standard deviation. The combined effect of ϵ and CV on P_{aval} is illustrated in Figure 4c. Again, the strong influence of ϵ for values lower than ≈ 4 m is clear and for values of $\epsilon < 1$ m, the CV has almost no influence due to the important smoothing effect. Indeed, in this case, as ϵ is much smaller than $\Lambda (= 1.1$ m), the variability in weak layer strength is averaged out due to stress redistributions by the elasticity of the slab. For large values of ϵ , CV mainly determines the changes in avalanche probability.

3.4. Influence of Slab Elasticity

As previously shown, an increase in elasticity (decreasing Young's modulus E) implies a decrease of both the knock-down and smoothing functions f_1 and f_2 (Figure 3). However, for a slope that is stable on average ($\rho ghF - f_1 \langle c \rangle < 0$), the two functions affect slope stability in opposite ways. An increase in f_1 with increasing E means an increase of stability since the apparent cohesion $f_1 \langle c \rangle$ increases. This can be well understood for the case of a single crack inside the WL for which the elasticity of the slab causes the stress at the tip of the crack to be redistributed (Figure 5a, inset). The failure criterion will then be reached more quickly than for a completely rigid slab, for which there is no stress redistribution. This explains why the stress required to trigger the instability increases with E (Figure 5a). The effect of the smoothing function f_2 , on the other hand, is to enhance the stability for low values of E since the WL heterogeneity is smoothed out. To illustrate the overall effects of f_1 and f_2 on P_{aval} and thus to understand the global effect of slab elasticity on slope stability,

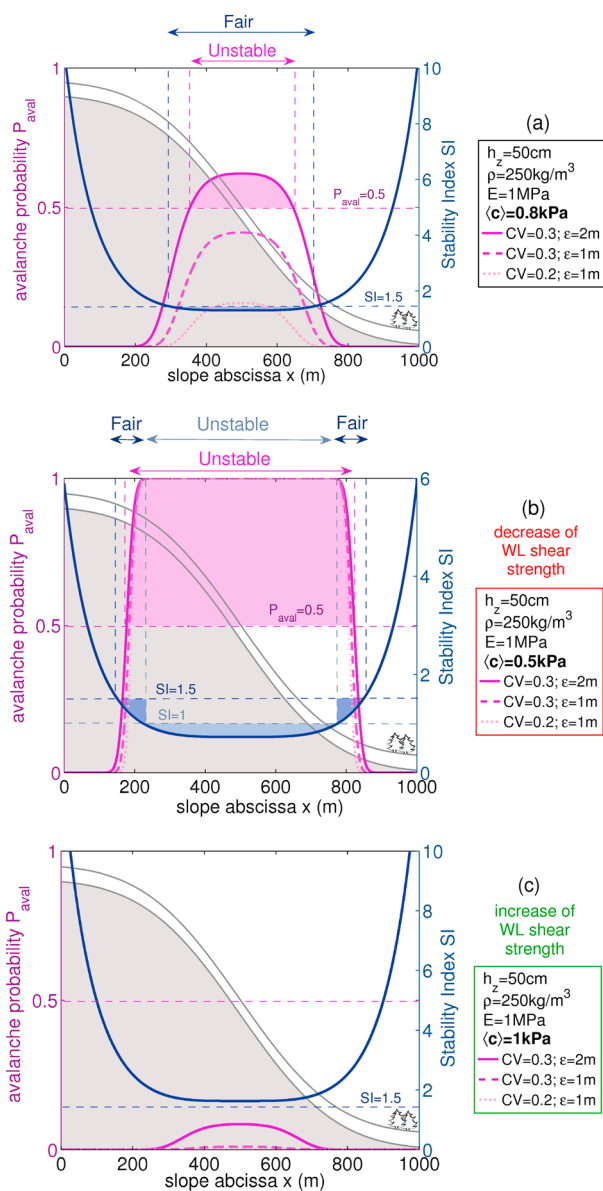


Figure 6. (a–c) Evaluation of the stability of a virtual slope (represented in grey with a white snowpack) of maximum angle $\theta = 45^\circ$ at $x = 500$ m, constant vertical slab depth $h_z = 0.5$ m ($h = h_z \cos \theta$), slab density $\rho = 250$ kg/m³ and a Young’s modulus $E = 1$ MPa using the following: (i) the classical stability index SI, i.e., the ratio between WL shear strength and shear stress due to the slab (blue curves) and (ii) the presented model that takes into account WL variations in shear strength (pink curves) for different scenarios of WL strength variations (different values of the coefficient of variation CV and correlation length ϵ).

(in SAFRAN-Crocus-MEPRA in France [Brun et al., 1992; Giraud, 1992] and in SNOWPACK in Switzerland [Lehning et al., 2004; Schweizer et al., 2006]), with our modeled avalanche probability for the simple case of a virtual snow slope (Figure 6). The slope has a maximum angle of 45° at $x = 500$ m, a constant slab depth of 50 cm, a slab density of 250 kg/m³, and a Young’s modulus $E = 1$ MPa. For an average cohesion of 800 Pa, the classical stability index is always above 1, suggesting a stable slope (Figure 6a). On the steep part of the slope the stability index is between 1 and 1.5, which is considered as “fairly stable.” The avalanche probability P_{aval} computed from equation (3), on the other hand, is larger than 0.5 for CV = 0.3. A decrease of

the avalanche probability is presented in Figure 5b as a function of the Young’s modulus of the slab for three values of the WL cohesion. Case #1, corresponds to the parametric analysis of the effect of E (constant density), whereas case #2 corresponds to a more realistic case in which the slab density was related to Young’s modulus by a power law fit of the data collected by Scapozza [2004]:

$$E(\rho) = 5.07 \times 10^9 \times \left(\frac{\rho}{\rho_{ice}}\right)^{5.13} \quad (10)$$

with $\rho_{ice} = 917$ kg/m³. However, in order to have comparable results, the weight of the slab was kept constant, i.e., the slab depth decreased as the density increased. For case #1, there is a clear decrease in P_{aval} with increasing E , thus stability increases with increasing stiffness. For case #2, on the other hand, the avalanche probability also decreases with increasing E but is lower than for case #1 for low values of the Young’s modulus ($E < 3$ MPa) and then becomes very slightly higher. The effect is more complicated in this more realistic case since for very low values of E , and thus low slab density, a very thick slab is required to obtain the same load. This implies weak knock-down ($f_1 \approx 1$) and large smoothing ($f_2 \rightarrow 0$) effects and thus an increase in stability compared to case #1. Overall, this result shows that a soft elastic slab facilitates failure initiation in the WL. Using different parameterizations to describe the relation between Young’s modulus and slab density would not significantly change this finding for a range of realistic slab density values.

3.5. Illustration of the Knock-Down Effect

In order to illustrate the knock-down effect and its importance for avalanche formation and forecasting, we compare the classical stability index, which is widely used for avalanche forecasting

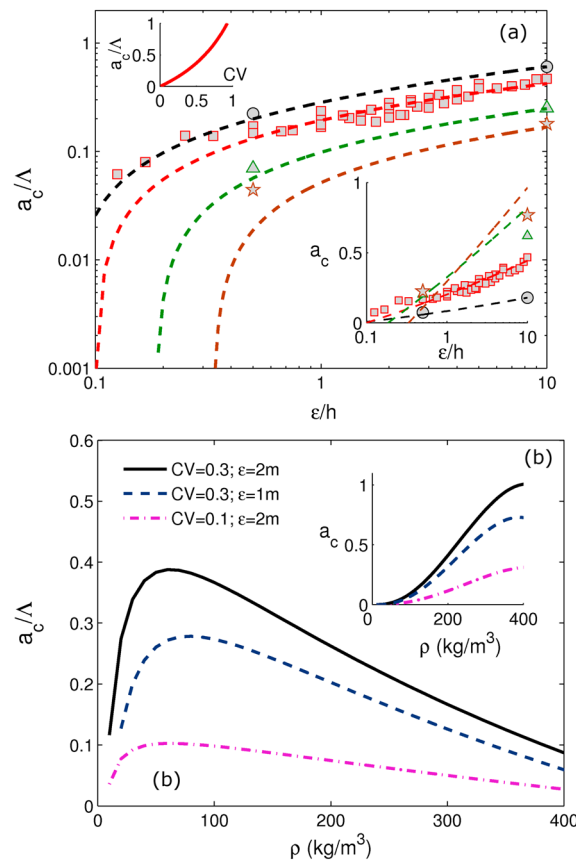


Figure 7. (a) Critical length (dimensionless and nondimensional) as a function of ϵ/h and as a function of the CV in inset. The different colors correspond to the different values of Young's modulus (black: $E = 0.1$ MPa, red: $E = 1$ MPa, green: $E = 10$ MPa, and brown: $E = 30$ MPa). The symbols are the results from the FE model, and the dashed lines are the fitted FE results (same legend as in Figure 3); (b) Critical length (dimensionless and nondimensional) as a function of slab's density and with a dependence of Young's modulus with ρ following the adjustment of Scapoza [2004] (equation (10)) and for a constant load.

and also in the inset of Figure 5a). It is not feasible to compute the critical length for each simulation with spatial variations of WL shear strength. We therefore assume that a_c follows the relationship given for a single crack (equation (6)), taking into account the average release depth obtained through the finite element simulations according to

$$\frac{a_c}{\Lambda} = \frac{1}{\langle h \rangle / h_{th}} - 1 = \frac{1}{f_1} - 1 \quad (11)$$

Hence, we can compute a_c as a function of ϵ/h , CV, and E . As expected, the critical length increases with increasing ϵ and CV, and decreases with increasing slab depth h due to smoothing effects (Figure 7a). Furthermore, the ratio a_c/Λ decreases with increasing E , but the critical length increases with increasing Young's modulus (since Λ increases with \sqrt{E}). Considering the relation between Young's modulus and snow density [Scapoza, 2004] (cf. case #2, section 3.4), the dimensionless critical length a_c/Λ peaks for a density of ≈ 60 kg/m³ after which it decreases with increasing density (Figure 7b), for all values of CV and ϵ . The critical length a_c increases with increasing slab density up to a density of ≈ 350 kg/m³, at which it stabilizes. As we showed above in section 3.4, soft slabs (low Young's modulus) are more prone to failure initiation under given loading conditions, resulting in lower values of the critical length a_c . The values of a_c

the CV and/or of the correlation length leads to a decrease of the avalanche probability—thus more stable conditions. Decreasing the average cohesion to 500 Pa leads to a stability index which is lower than 1 on the steep part of the slope (Figure 6b). Hence, this would be forecasted as an unstable slope. For this case, the avalanche probability is equal to 1 regardless of the value of the CV. Consequently, for the unstable case, both approaches lead to similar results. Finally, increasing the average cohesion to 1000 Pa (Figure 6c), the stability index predicts a slope which can be considered as completely stable ($SI > 1.5$). In this case, the avalanche probability also predicts a slope that is stable on average. However, for $CV = 0.3$ and a correlation length $\epsilon = 2$ m the avalanche probability P_{aval} is still almost 10%. This simple example highlights the need to account for spatial variability in WL shear strength and its knock-down effect on slope stability. Indeed, the WL heterogeneity coupled with the elasticity of the slab induces stress concentrations at the tip of the weaker zones which can in turn reach the failure criterion more easily. These effects can significantly change the stability prediction given by the classical stability index.

4. Application to the Evaluation of the Critical Length

4.1. From WL Heterogeneity to the Critical Length

Once a failure has been initiated inside the WL, it has to reach a critical length, denoted by a_c , to become self-propagating (an illustration is given in the supporting information

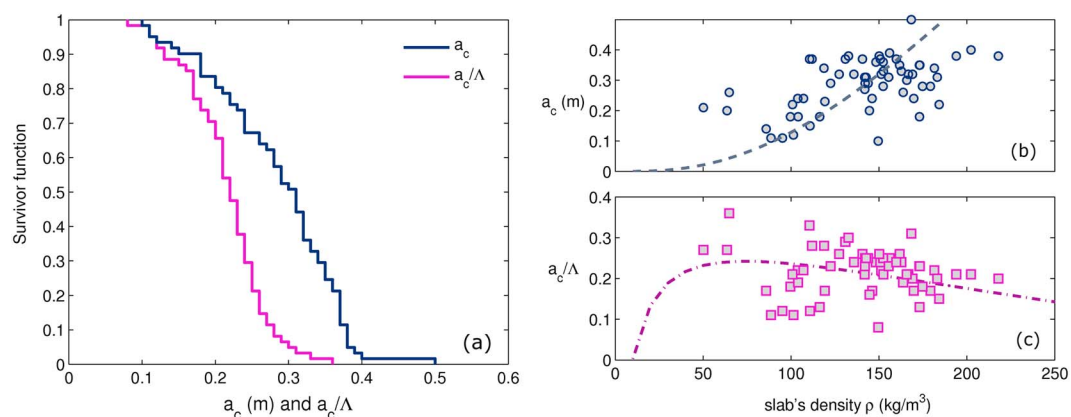


Figure 8. (a) Survivor functions of the critical length $P(\geq a_c)$ and dimensionless critical length $P(\geq a_c/\Lambda)$ from 62 propagation saw tests (PSTs) near Davos [Reuter and Schweizer, 2012]. The survivor function corresponds to the probability of having a value higher or equal than a threshold, represented in abscissa. (b) Critical length and (c) dimensionless critical length as a function of the average slab density for PST measurements. The dotted lines correspond to the model prediction for $CV = 25\%$, $\epsilon = 1.5$ m, and $\langle c \rangle = 300$ Pa corresponding to an average specific fracture energy $G_{II} = 0.21$ J/m².

are typically between 5 and 50 cm for realistic values of the parameters which is consistent with field measurements [Schweizer, 1999; Gauthier and Jamieson, 2008; McClung, 2011; Ross and Jamieson, 2012; Reuter and Schweizer, 2013]. The dimensionless critical length a_c/Λ ranges between 0.05 and 0.35. This is a very interesting result since, as shown in Appendix B, for values of a_c/Λ lower than approximately 0.4, the critical length is almost independent of the approach which is considered (strength of material or fracture mechanics) and the assumptions (presence or absence of collapse) to be used. For $a_c/\Lambda > 0.5$, thus for large crack lengths and/or very low slab density (implying high elasticity, i.e., low Young's modulus), the purely mechanical and fracture mechanical approaches lead to substantially different results, difference which is further amplified if WL collapse is considered.

4.2. Comparison With Field Data

In this section, we compare our modeled critical lengths to those obtained from 62 propagation saw tests (PSTs) [Reuter and Schweizer, 2012]

4.2.1. PST Data

The propagation saw test was concurrently developed by Gauthier and Jamieson [2006] and Sigrist and Schweizer [2007]. Gauthier and Jamieson [2008] showed that it is a good indicator for crack propagation propensity. We made measurements near Davos, Switzerland, during the winters of 2009/2010 and 2010/2011 for different aspects, slope angles (from 15 to 30°), slab depths (from 20 to 60 cm), and slab densities (from 120 to 270 kg/m³). The distribution of the critical length a_c obtained from these measurements is shown in Figure 8a as well as the dimensionless critical length a_c/Λ . To compute Λ , the WL cohesion is required but was not directly measured (the shear stiffness k_s of the WL is equal to the ratio between WL shear strength and a characteristic peak tangential displacement, see Gaume et al. [2013a], for more details). Hence, WL cohesion was derived from the specific fracture energy G_{II} according to equation (B7) in Appendix B. The specific fracture energy was determined using finite element modeling [Sigrist, 2006; Sigrist and Schweizer, 2007]. Furthermore, since the PSTs were performed from the lower edge of the system, the critical lengths obtained from the PSTs were compared to half the critical length obtained from the model (which considers a crack in the middle of the weak layer). This assumption was corroborated by recent field measurements [Bair et al., 2014]. Note, however, that Sigrist and Schweizer [2007] showed, on the basis of the anticrack model [Heierli et al., 2008], that the ratio between the critical length obtained from a standard PST (from the edge) and a centered one should be a little less than 1/2 (around 0.41).

4.2.2. Analysis and Model-Data Comparison

The largest measured values of the dimensionless critical length were typically lower than 0.35 (0.5 m for the critical length; Figure 8a), confirming the usefulness of our approach to investigate slope stability (Appendix B). The values of a_c and a_c/Λ are shown as a function of slab density in Figures 8b and 8c. The critical length a_c obtained from the PSTs tends to increase with increasing density (Figure 8b), whereas the dimensionless critical length a_c/Λ decreases with increasing density (Figure 8c). These relations are in

accordance with the model predictions (dashed lines in Figures 8b and 8c). Of course, the measurements were made for different snowpack conditions and thus different WL heterogeneities, which partly explain the important scatter in the data. Nevertheless, our model is in reasonable agreement with the global trend of the field data.

5. Discussion

The proposed approach based on a mechanical-statistical model of the slab-WL system allows to quantitatively link snowpack properties and their variations to avalanche release probability and thus slope stability for spontaneous avalanches. However, when interpreting the outcome of the parametric analysis, one should keep in mind that for snow the mechanical parameters are often linked, which may lead to more complex interactions than presented here. For instance, we showed that the dependence of the avalanche probability on the Young's modulus of the slab is different if the Young's modulus varies with density rather than assuming the two variables to be independent (Figure 5b). Considering this interaction, the critical length required for crack expansion in the weak layer computed from heterogeneity and snowpack properties was in good agreement with field data (Figures 8b and 8c). This opens a new interesting perspective for analyzing the outcome of experiments and, hence, better understanding avalanche release processes.

The present study shares some similarities with that by *Fyffe and Zaiser* [2004] who used a cellular automaton model to investigate the influence of variations in WL shear strength on slope stability. These authors focused mainly on the influence of the coefficient of variation CV. While qualitatively their results showed similar trends for the evolution of the knock-down function with CV, quantitatively the results were very different. *Chiaia and Frigo* [2009] also used a related approach based on a scale-invariant fractal model to evaluate the conditions of failure of a slab-WL system taking into account a random distribution of the shear strength. They showed, in particular, how complex local interactions and failures at small scales may lead to catastrophic failure at the macroscopic scale. However, in these two studies, the elasticity of the slab was not completely taken into account and stress redistribution effects were oversimplified. Hence, their results can only be applied to cases in which the correlation length is smaller than the slab depth. Besides, the scale-invariance assumption postulated in these approaches is refuted when slab elasticity is accounted for, as the characteristic length of the system Λ appears in the equilibrium equations, as already noted by *Chiaia et al.* [2008]. Nevertheless, as shown by *Gaume et al.* [2013a], the existence of this characteristic length Λ still permits to obtain scale-free (power law) distributions of avalanche release depths, as observed in the field.

Finally, let us point out that size effects, which are of crucial importance for avalanche release [*Bazant et al.*, 2003], are indirectly addressed in our model. The size effect is defined as the effect of the system size (in our case, the slab depth h) on the fracture toughness or on the strength of the material. However, snow slabs of different depths also generally have very different properties at their base, due to densification and sintering. Hence, one should distinguish between the structural size effect which induces a decrease of the strength with the sample size and the material size effect [*Bazant et al.*, 2003]. For snow, existing data suggest a strong increase of the shear strength with the slab depth. *Bazant et al.* [2003] and *McClung and Schweizer* [2006] reported the shear strength as a function of the slab depth h (normal to the slope) for 116 avalanches (data described in *Perla* [1977]) and evidenced a power law dependence: $\tau_p \sim h^{1.30}$. Yet as already emphasized by *Bazant et al.* [2003], "available field data are too limited to allow precise conclusions" about the origin of the size effect and the structural and material contributions. In our approach, we argue that the overall size effect is taken into account through the Mohr-Coulomb criterion of the WL. Indeed, the shear strength τ_p of the WL is a function of the slab depth through the normal stress $\sigma_n = \rho gh \cos \theta$ due to the load of the slab: $\tau_p = c + \sigma_n \tan \phi$. Besides, *McClung* [2009] found that the slab depth is also generally correlated to slab density according to $\rho \sim 225 \times h^{0.24}$. If this relation is reported into Mohr-Coulomb's criterion, the shear strength would vary as $\tau_p \sim c + 2.2 \times 10^{-3} h^{1.24} \tan \phi$. This dependency with h is very close to that reported by *Bazant et al.* [2003] (exponent 1.3 versus 1.24) and also very nicely fits the data presented in their paper (for a friction angle $\phi = 30^\circ$ and a cohesion $c = 100$ Pa). Hence, the results of our model could even be slightly improved if the relationship between slab depth and slab density was accounted for. As mentioned in Appendix B, strength of material and fracture mechanics approaches lead to very similar results up to a certain limit. However, in classical linear elastic fracture mechanics, size effects are generally taken into account empirically, whereas they are indirectly taken into account through the constitutive and

failure behavior in strength of material approaches, which are in that sense, more powerful, provided that the failure criterion is known.

6. Conclusions

As spatial variations of weak layer mechanical properties strongly influence avalanche formation and thus slope stability [Schweizer *et al.*, 2008], we presented a method based on stochastic finite element simulations to link slope stability to weak layer (WL) spatial variability for natural releases. The model considers spatial variations of WL shear strength and stress redistribution by the elasticity of the overlying slab.

Our results showed two main effects of weak layer spatial variability. First, a knock-down effect which tends to reduce the apparent cohesion of the WL and thus slope stability. This effect is due to stress concentrations at the tip of the weakest zones, which can thus more easily reach the failure criterion. This effect depends on three factors: (i) the ratio between the correlation length ϵ and the slab depth h , (ii) the coefficient of variation of the heterogeneity CV, and (iii) the Young's modulus E of the slab.

Second, a smoothing effect tends to reduce the apparent variability. This effect depends on the Young's modulus of the slab E and on the ratio between the correlation length ϵ , and the characteristic elastic length of the system Λ . By combining the two effects, the avalanche probability can be derived as a function of the characteristics of the WL spatial variation and the relevant slab properties. It was especially shown that strong WL heterogeneities (high values of the correlation ϵ and of the coefficient of variation CV) as well as low slab densities and depths were facilitating failure initiation.

Besides, the critical length for crack expansion has been determined by comparing our results to the case of a simple crack. We showed that the critical length a_c is an increasing function of the coefficient of variation and correlation length of the WL variation and also decreases with increasing slab density. However, the critical length decreases with increasing slab depth in agreement with previous experimental studies. Moreover, we have shown that our model could reasonably reproduce the critical length obtained from 62 propagation saw tests.

Furthermore, we also highlighted the crucial importance of the characteristic elastic length of the system Λ which depends on both the slab and the WL properties to characterize the complex processes at play in slab avalanche release. In particular, this length, coupled with the other important parameters of the system, namely, the correlation length ϵ , the slab depth h , and the Young's modulus E of the slab, allowed us to explain and reproduce all our FE simulations and to compute the avalanche probability for different snowpack conditions. In practice, elastic properties of snow may be derived from density [Scapozza, 2004] which enables to compute Λ . Then, as shown in section 4.1, the correlation length ϵ and coefficient of variation CV can be computed from the critical length obtained from PST experiments allowing ultimately to compute the knock-down and smoothing functions f_1 and f_2 and thus refining classical stability predictions.

Finally, for practical application in avalanche forecasting and a straightforward implementation to a numerical snow cover model, for example, SNOWPACK, the link between spatial variations of snowpack properties and the underlying meteorological conditions is required as spatial variability is the result of the complex interaction between mountain weather, such as wind and solar radiation, and terrain.

Appendix A: Fits of the Knock-Down and Smoothing Functions f_1 and f_2

In the following we explain how the fits of the knock-down function f_1 and smoothing function f_2 (Figure 3) were obtained and provide their expressions. The procedure was to find a relevant combination of dimensionless numbers of the system which explains all the values of f_1 and f_2 obtained using the finite element method for all the simulated parameters, namely, the correlation length ϵ , the slab depth h , the coefficient of variation CV, and the Young's modulus of the slab E . After several tests (using the linear least square method), the following three dimensionless parameters, all scaled using the characteristic elastic length Λ , were selected in addition to the coefficient of variation CV: ϵ/Λ , h/Λ , and $E/(\rho g \Lambda)$. A power law combination of all these parameters allowed us to explain the results from all the FE simulations (Figure A1). Figure A1a shows that all f_1 values collapse on the same master curve when it is represented against the quantity $V_1 = (\epsilon/\Lambda)(h/\Lambda)^{-2}(E/(\rho g \Lambda))^{-3}$. Similarly, all f_2 values are explained by the quantity $V_2 = (\epsilon/\Lambda)(E/(\rho g \Lambda))^{1.2}$ (Figure A1b).

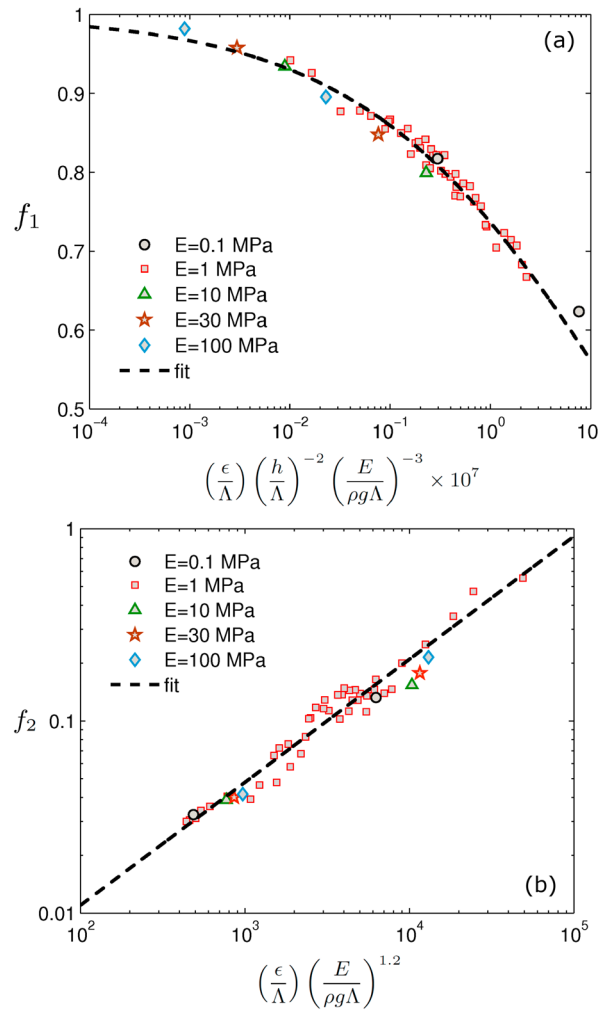


Figure A1. (a) Knock-down function f_1 as a function of the dimensionless parameter $V_1 = (\epsilon/\Lambda) (h/\Lambda)^{-2} (E/(\rho g \Lambda))^{-3}$ for all the simulated parameters. The dashed line is a fit of the form $f_1 = 1/(1 + \alpha_1 V_1^{\beta_1})$ adjusted using the linear least square method ($R^2 = 0.973$). (b) Smoothing function f_2 as a function of the dimensionless parameter $V_2 = (\epsilon/\Lambda) (E/(\rho g \Lambda))^{1.2}$ for all the simulated parameters. The dashed line is a power law fit of the form $f_2 = \alpha_2 V_2^{\beta_2}$ adjusted using the linear least square method ($R^2 = 0.93$).

Finally, the complete expression of the knock-down function f_1 is given by

$$f_1(V_1) = 1 - \left[1 - \frac{1}{1 + \alpha_1 V_1^{\beta_1}} \right] \cdot \frac{CV}{0.3}, \quad (A1)$$

with $\alpha_1 = 84.5$, $\beta_1 = 0.339$, and $\rho = 250 \text{ kg/m}^3$. The smoothing function f_2 is given by

$$f_2(V_2) = \alpha_2 V_2^{\beta_2}, \quad (A2)$$

with $\alpha_2 = 5.76 \times 10^{-4}$ and $\beta_2 = 0.64$. This result highlights, in particular, and as already pointed out previously [Chiaia et al., 2008; Gaume et al., 2013a], the crucial importance of the characteristic elastic length of system Λ which depends on both the slab and WL properties to assess the conditions for slab avalanche release.

However, in the text, it was easier to explain the results by showing the knock-down and smoothing functions f_1 and f_2 as a function of the variables ϵ/h , ϵ/Λ , CV , and E .

Appendix B: Comparison Between Fracture Mechanics and Strength of Material Methods to Evaluate the Critical Length

Different approaches have been proposed to compute the critical length required for a self-propagating crack. These approaches, relying on different assumptions and physical ingredients, have recently been applied to dry snow slab avalanche release to characterize the propagation propensity of a slab-WL system:

1. The classical fracture mechanics approach [Griffith, 1920] focuses on the growth of a crack inside a homogeneous material. The crack propagates when the elastic strain energy stored in the material balances the fracture energy required to destroy the cohesion along the crack;
2. The anticrack model proposed by Heierli et al. [2008] considers a slab-WL system and assumes that the collapse of the WL is due to the change in strain and gravitational potential energy (bending) of the slab. Besides, the WL is assumed to be completely rigid;
3. Strength of material approaches solve the equilibrium equations of a slab-WL system in the presence of a single crack within the WL [Chiaia et al., 2008; Gaume et al., 2013a]. Stress concentrations occur at the tip of the crack which propagates when the failure criterion is reached. These approaches have highlighted a characteristic length of the system Λ , which depends on the properties of both the slab and the WL and which controls the decrease of the shear stress around the crack.

Hence, the objective of this appendix is to compare the strain energy required for propagation of a single crack of half-length a using these different approaches in order to evaluate the relevance of our proposed model for reproducing field observations. It can easily be shown that the strain energy required for crack

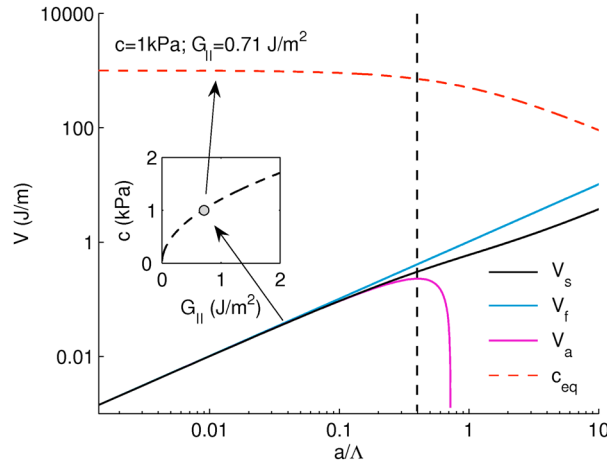


Figure B1. Strain energy required for crack expansion as a function of the ratio between the crack size a and the characteristic elastic length Λ for the three different approaches presented: strength of material with shear quasi-brittle WL (V_s , in black), classical fracture mechanics (V_f , in blue), anticrack model (V_a , in magenta). The red dashed line corresponds to the equivalent cohesion given by equation (B7) which is valid for short cracks. The black dashed line corresponds to $a/\Lambda = 0.4$. The following parameters were used: $h = 0.35$ m, $\theta = 35^\circ$, $E = 1$ MPa, $\nu = 0.2$, $c = 1$ kPa, and $G_{II} = 0.71$ J/m².

expansion in a quasi-brittle WL underlying a cohesive elastic slab can be expressed as follows [Chiaia et al., 2008]:

$$V_s(a) = \frac{(\tau_r - \tau)^2}{3E'h} [(a + \Lambda)^3 - \Lambda^3] = \frac{(\tau_r - \tau_p)^2 [(a + \Lambda)^3 - \Lambda^3]}{3E'h \left(1 + \frac{a}{\Lambda}\right)^2} \quad (B1)$$

Then, according to fracture mechanics [Griffith, 1920], the fracture energy required for crack propagation is the product between the specific fracture energy G_{II} and the size of the crack:

$$V_f(a) = 2G_{II}a \quad (B2)$$

Finally, if the WL normal collapse is considered using the anticrack model of Heierli et al. [2008], the total strain energy can be expressed as follows:

$$V_a(a) = 2G_{II}a - \frac{\gamma \pi (\rho g h a)^2}{2E'} - \frac{(\rho g h)^2 a^3}{3E'h} (\beta_1 \sin^2 \theta + \beta_2 \cos^2 \theta), \quad (B3)$$

where

$$\beta_1 = 1 + 9 \frac{\eta^2}{3\eta^2 + 4(a/h)^2}, \quad (B4)$$

and

$$\beta_2 = 3\eta^2 + \frac{4}{5} \frac{(a/h)^2 \left(\frac{9}{4}\eta + \frac{a}{h}\right)}{\eta + \frac{a}{h}} \quad (B5)$$

and $\gamma = 2.331$, $\eta = E'/(3kG)$, $k = 5/6$, $G = E/(2(1 + \nu))$.

Note that equation (B3) is only valid for $a < l_0$, l_0 being the length for which the bended slab is in contact with the collapsed WL. This length l_0 can be computed from Timoshenko and Goodier [1970]. Above this length, the strain energy has the same form as for a shear quasi-brittle WL.

Besides, the classical stress criterion can be related to the fracture mechanics approach by computing the specific fracture energy G_{II} by differentiating equation (B3):

$$G_{II} = \frac{\partial V_s(a)}{\partial (2a)} \quad (B6)$$

Hence, for short cracks, one can compute directly the shear strength of the WL as a function of the specific fracture energy as follows:

$$c = \frac{\sqrt{2hG_{II}E'}}{a + \Lambda} \quad (B7)$$

For these different approaches, the strain energy required crack expansion has been represented as a function of the ratio between the crack size a and the characteristic length of the system Λ (Figure B1). The relation between WL cohesion c and the specific fracture energy G_{II} is shown in the inset. The strain energy from the strength of material approach has been computed considering a cohesion value $c = 1$ kPa that matches the value of $G_{II} = 0.71$ J/m² used for the fracture and anticrack approaches according to

equation (B7). Hence, for short crack length, typically for a/Λ lower than ≈ 0.4 , all these different approaches (relying on different assumptions) lead to the same strain energy values. Above this line, the values starts to be significantly different since the strain energy required to expand a crack in a quasi-brittle WL starts to increase more strongly with the crack size, whereas the strain energy based on the anticrack model decreases drastically with increasing crack size until the slab reaches the collapsed WL ($a = l_0$). With the parameterization used, the length l_0 is approximately equal to 0.69 m ($l_0/\Lambda \approx 0.9$). The equivalent cohesion computed from equation (B7) was also represented in Figure B1 as a function of a/Λ . It shows that below $a/\Lambda \approx 0.4$, the equivalent cohesion is almost constant equal to 1 kPa and then starts to decrease with a/Λ .

The comparison described above suggests that for low values of the critical length, the proposed approach which solves the equilibrium equations of the slab-WL system in the presence of a crack within the WL and taking into account a simple shear stress criterion leads to similar results as those obtained with fracture mechanics and anticrack modeling approaches. More than that, this strength of material approach can even be seen more complete than that of classical fracture mechanics which assumes a homogeneous material. Indeed, taking into account the layering of the system has the consequence that the specific fracture energy G_{II} is not constant but depends on a/Λ beyond a certain value of this parameter ($a/\Lambda > 0.4$).

Notation

a	crack length (m)
a_c	critical crack length (m)
c	WL cohesion (Pa)
$\langle c \rangle$	WL average cohesion (Pa)
CV	coefficient of variation of WL heterogeneity
E	slab Young's modulus (Pa)
ϵ	correlation length of WL heterogeneity (m)
f_1	knock-down function
f_2	smoothing function
G_{II}	specific fracture energy (J/m^2)
h	slab depth measured normal to the slope (m)
$\langle h \rangle$	average release depth (m)
h_{th}	theoretical release depth (m)
k_s	WL interfacial shear stiffness (Pa/m)
L	length of the system (m)
Λ	characteristic elastic length (m)
μ	WL friction coefficient
ν	slab Poisson's ratio
P_{aval}	avalanche release probability
ϕ	WL friction angle
θ	slope angle
ρ	slab density (kg/m^3)
ρ_{ice}	ice density (kg/m^3)
σ_c	WL cohesion standard deviation (Pa)
σ_h	release depth standard deviation (m)
σ_n	normal stress due to the slab (Pa)
σ_∞	release depth standard deviation for $E \rightarrow \infty$ (m)
SI	stability index
τ_g	shear stress due to the slab (Pa)
τ_{max}	maximum shear stress at the crack tip (Pa)
τ_p	WL shear strength (Pa)
τ_r	residual shear stress (Pa)
$\langle \tau_p \rangle^*$	average apparent shear strength (Pa)
V_a	strain energy for the anticrack model (J/m)
V_s	strain energy for the strength of material approach (J/m)
V_s	strain energy for the fracture mechanics approach (J/m)

Acknowledgments

Document data are available on request by sending an email to Johan Gaume at johan.gaume@sif.ch. We also wish to express our gratitude to B. Jamieson, two anonymous reviewers, and to the Scientific Editor M. Louge for their insightful and constructive comments.

References

- Bair, E., R. Simenhois, A. van Herwijnen, and K. Birkeland (2014), The influence of edge effects on crack propagation in snow stability tests, *The Cryosphere*, 8, 1407–1418, doi:10.5194/tc-8-1407-2014.
- Bazant, Z. P., G. Zi, and D. McClung (2003), Size effect law and fracture mechanics of the triggering of dry snow slab avalanches, *J. Geophys. Res.*, 108, 2119, doi:10.1029/2002JB001884.
- Bellaire, S., and J. Schweizer (2011), Measuring spatial variations of weak layer and slab properties with regard to snow slope stability, *Cold Reg. Sci. Technol.*, 65(2), 234–241.
- Birkeland, K., B. Hansen, and R. Brown (1995), The spatial variability of snow resistance on potential avalanche slopes, *J. Glaciol.*, 41(137), 183–189.
- Blanchet, J., and M. Lehning (2010), Mapping snow depth return levels: Smooth spatial modeling versus station interpolation, *Hydrol. Earth Syst. Sci. Discuss.*, 7, 6129–6177.
- Brun, E., P. David, M. Sudul, and G. Brunot (1992), A numerical model to simulate snow-cover stratigraphy for operational avalanche forecasting, *J. Glaciol.*, 38(128), 13–22.
- Chiaia, B., and B. Frigo (2009), A scale-invariant model for snow slab avalanches, *J. Stat. Mech.*, 2009(2), P02056, doi:10.1088/1742-5468/2009/02/P02056.
- Chiaia, B., P. Cornetti, and B. Frigo (2008), Triggering of dry snow slab avalanches: Stress versus fracture mechanical approach, *Cold Reg. Sci. Technol.*, 53, 170–178.
- Durand, Y., M. Latenser, G. Giraud, P. Etchevers, B. Lesaffre, and L. Mérindol (2009), Reanalysis of 44 yr of climate in the French Alps (1958–2002): Methodology, model validation, climatology, and trends for air temperature and precipitation, *J. Appl. Meteorol. Climatol.*, 48, 429–449, doi:10.1175/2008JAMC1808.1.
- Eckert, N., C. Coleou, H. Castebrunet, M. Deschates, D. Giraud, and J. Gaume (2010), Cross-comparison of meteorological and avalanche data for characterising avalanche cycles: The example of December 2008 in the eastern part of the French Alps, *Cold Reg. Sci. Technol.*, 64, 119–136.
- Failletaz, J., F. Louchet, and J. Grasso (2004), Two-threshold model for scaling laws of noninteracting snow avalanches, *Phys. Rev. Lett.*, 93(20), 208,001, doi:10.1103/PhysRevLett.93.208001.
- Fyffe, B., and M. Zaiser (2004), The effects of snow variability on slab avalanche release, *Cold Reg. Sci. Technol.*, 40, 229–242.
- Fyffe, B., and M. Zaiser (2007), Interplay of basal shear fracture and slab rupture in slab avalanche release, *Cold Reg. Sci. Technol.*, 49, 26–38.
- Gaume, J., G. Chambon, N. Eckert, and M. Naaim (2012), Relative influence of mechanical and meteorological factors on avalanche release depth distributions: An application to French Alps, *Geophys. Res. Lett.*, 39, L12401, doi:10.1029/2012GL051917.
- Gaume, J., G. Chambon, N. Eckert, and M. Naaim (2013a), Influence of weak-layer heterogeneity on snow slab avalanche release: Application to the evaluation of avalanche release depths, *J. Glaciol.*, 59(215), 423–437.
- Gaume, J., G. Chambon, N. Eckert, and M. Naaim (2013b), Mapping extreme snowfalls in the French Alps using max-stable processes, *Water Resour. Res.*, 49, 1079–1098, doi:10.1002/wrcr.20083.
- Gauthier, D., and B. Jamieson (2006), Towards a field test for fracture propagation propensity in weak snowpack layers, *J. Glaciol.*, 52(176), 164–168.
- Gauthier, D., and B. Jamieson (2008), Evaluation of a prototype field test for fracture and failure propagation propensity in weak snowpack layers, *Cold Reg. Sci. Technol.*, 51(2), 87–97.
- Giraud, G. (1992), Mepra: An expert system for avalanche risk forecasting, paper presented at International Snow Science Workshop, Colorado Avalanche Information Center, Denver Colo., Breckenridge, Colo. 4–8 Oct.
- Griffith, A. (1920), The phenomena of rupture and flow in solids, *Philos. Trans. R. Soc. A*, 221, 163–198.
- Heierli, J., P. Gumbsch, and M. Zaiser (2008), Anticrack nucleation as triggering mechanism for snow slab avalanches, *Science*, 321, 240–243, doi:10.1126/science.1153948.
- Jamieson, B., and C. Johnston (1993), Rutschblock precision, technique variations and limitations, *J. Glaciol.*, 39(133), 666–674.
- Jamieson, J., and C. Johnston (2001), Evaluation of the shear frame test for weak snowpack layers, *Ann. Glaciol.*, 32, 59–69.
- Kronholm, K., and J. Schweizer (2003), Snow stability variation on small slopes, *Cold Reg. Sci. Technol.*, 37(3), 453–465.
- Landry, C., K. Birkeland, K. Hansen, J. Borkowski, R. Brown, and R. Aspinall (2004), Variations in snow strength and stability on uniform slopes, *Cold Reg. Sci. Technol.*, 39(2-3), 205–218.
- Lehning, M., C. Fierz, B. Brown, and B. Jamieson (2004), Modeling snow instability with the snow-cover model SNOWPACK, *Ann. Glaciol.*, 38(1), 331–338.
- McClung, D. (1979), Shear fracture precipitated by strain softening as a mechanism of dry slab avalanche release, *J. Geophys. Res.*, 84(B7), 3519–3526.
- McClung, D. (2009), Dry snow slab quasi-brittle fracture initiation and verification from field tests, 114, F01022, doi:10.1029/2007JF000913.
- McClung, D. (2011), Analysis of critical length measurements for dry snow slab weak-layer shear fracture, *J. Glaciol.*, 57(203), 557–566.
- McClung, D., and J. Schweizer (2006), Fracture toughness of dry snow slab avalanches from field measurements, *J. Geophys. Res.*, 111, F04008, doi:10.1029/2005JF000403.
- Mellor, M. (1975), *A Review of Basic Snow Mechanics*, Publ. 114 pp. 251–291, Int. Assoc. of Hydrol. Sci. (IAHS), Geneva, Switz.
- Meunier, M., and C. Ancey (2004), Towards a conceptual approach to predetermining high-return-period avalanche run-out distances, *J. Glaciol.*, 50(169), 268–278.
- Perla, R. (1977), Slab avalanche measurements, *Can. Geotech. J.*, 14(2), 206–213.
- Reuter, B., and J. Schweizer (2012), The effect of surface warming on slab stiffness and the fracture behavior of snow, *Cold Reg. Sci. Technol.*, 83, 30–36.
- Reuter, B., and J. Schweizer (2013), Linking weather conditions to snow property variations, in *Proceedings International Snow Science Workshop*, edited by F. Naaim-Bouvet, Y. Durand, and R. Lambert, pp. 61–64, Int. Snow Sci. Workshop, Grenoble, France.
- Ross, C. K., and B. Jamieson (2012), The propagation saw test: Slope scale validation and alternative test methods, *J. Glaciol.*, 58(208), 407–416.
- Scapozza, C. (2004), Entwicklung eines dichte- und temperaturabhängigen Stoffgesetzes zur Beschreibung des visko-elastischen Verhaltens von Schnee, PhD thesis, ETH Zürich, Zürich, Switzerland.
- Schweizer, J. (1999), Review of dry snow slab avalanche release, *Cold Reg. Sci. Technol.*, 30, 43–57.
- Schweizer, J., B. Jamieson, and M. Schneebeli (2003), Snow avalanche formation, *Rev. Geophys.*, 41(4), 1016, doi:10.1029/2002RG000123.
- Schweizer, J., S. Bellaire, C. Fierz, M. Lehning, and C. Pielmeier (2006), Evaluating and improving the stability predictions of the snow cover model SNOWPACK, *Cold Reg. Sci. Technol.*, 46(1), 52–59.

- Schweizer, J., K. Kronholm, J. Jamieson, and K. Birkeland (2008), Review of spatial variability of snowpack properties and its importance for avalanche formation, *Cold Reg. Sci. Technol.*, *51*(2-3), 253–272.
- Sigrist, C. (2006), Measurements of fracture mechanical properties of snow and application to dry snow slab avalanche release, PhD thesis, ETH Zürich, Zürich, Switzerland.
- Sigrist, C., and J. Schweizer (2007), Critical energy release rates of weak snowpack layers determined in field experiments, *Geophys. Res. Lett.*, *34*, L03502, doi:10.1029/2006GL028576.
- Timoshenko, S., and J. Goodier (1970), *Theory of Elasticity*, vol. 37, 888 pp., McGraw-Hill, New York.
- van Herwijnen, A., and J. Heierli (2009), Measurements of crack-face friction in collapsed weak snow layers, *Geophys. Res. Lett.*, *36*, L23502, doi:10.1029/2009GL040389.